Machine-precision fracture mechanics evaluations with the consistent boundary element method

Ney Augusto Dumont[1], Osmar Alexandre do Amaral Neto[1]

[1]*Dept. of Civil and Environmental Engineering, Pontifical Catholic University of Rio de Janeiro*
Rua Marquês de São Vicente, 225, 22451-900, Rio de Janeiro, Brazil
dumont@puc-rio.br, osmaralexandre22@hotmail.com

Abstract. As hitherto proposed in the technical literature, the boundary element modeling of cracks is best carried out resorting to a hypersingular fundamental solution – in the frame of either the so-called dual formulation or the displacement discontinuity approach –, since with Kelvin's fundamental solution it would not be possible to deal with the ensuing numerical and topological issues. A more natural approach would be the direct representation of the crack tip singularity in terms of generalized Westergaard stress functions, as already proposed in the frame of the hybrid boundary element method. Quite recently, we have been able to demonstrate that the conventional boundary element formulation is in fact able to precisely represent high-stress gradients and deal with extremely convoluted topologies provided only that the problem's integrals be properly evaluated, which has turned out to be the case. The reference literature on the present subject is briefly outlined along with the paper, which includes the simplest scheme of evaluating stress intensity factors in terms of crack tip opening displacements as a viable alternative to the J-integral. We propose that independently of configuration a cracked structure be geometrically represented as it would appear in real-world laboratory experiments, with crack openings in the range of micrometers or even nanometers, which would still be mathematically feasible – albeit not mechanically. In fact, machine precision evaluation of all quantities may be always achieved and stress results consistently obtained at interior points arbitrarily close to crack tips. The present developments apply to two-dimensional problems. Some numerical illustrations show that highly accurate results are obtained for cracks represented with just a few quadratic, generally curved, boundary elements – and a few Gauss-Legendre integration points per element. We also investigate how different simulations of the crack tip shape affect results, which turn out to be more accurate with the use of higher-order, such as quartic, boundary elements.

Keywords: Boundary elements, fracture mechanics, machine-precision integration

1 Introduction

The study of fracture mechanics phenomena was inaugurated by Inglis [1] in the year 1913. Griffith [2] introduced in 1920 thermodynamics concepts to formulate a fracture mechanics theory based on *energy balance*, extended by Irwin [3] to metals with the concept of *energy release rate* and, on the basis of the developments by Westergaard [4], also the proposition of *stress intensity factors* (SIF) [5]. The concept of a *crack opening displacement* (COD) was proposed by Dugdale [6] in 1960 to account for yielding at the crack tip. In the year 1968, Rice [7] showed that the energy release rate may be obtained by means of the *J-integral*. The application of these concepts to a practical problem depends on the adequate evaluation of the stress state around a crack tip. The first boundary element development in the field may be attributed to Cruse [8] in the year 1971.

The second author and previous collaborators have already in part successfully arrived at an attempt on the basis of the *hybrid boundary element method* to adequately represent the stress field around a crack tip in terms of Williams' series as well as of generalizations of Westergaard's [4] stress functions [9–11].

More recently, a consistent formulation – actually a both conceptually and numerically long due correction – of the conventional, *collocation boundary element method* (CBEM) was proposed [12, 13], according to which a convergence theorem could be envisaged and the evaluation of results has turned out achievable within machine precision for internal points arbitrarily close to an elastic body's boundary regardless of topology issues.

The numerical implementation considers arbitrarily high-order boundary elements for 2D bodies of any shape and topology as well as flat boundary elements of a three-dimensional body. The application of this consistent formulation to 2D fracture mechanics problems was the subject of the second author's M.Sc. thesis [14], which showed that a generically curved crack may be numerically simulated exactly as if in a real-life experimentation, with the faces distinctly modelled for arbitrarily small openings as long as the continuum mechanics is dimmed applicable[15].

This short paper is a continuation of Dumont and Amaral Neto [16]: readers are referred to it for a brief introduction to the problem and for evaluations using the J-integral for cracks in the open domain as well as in the case of an inclined edge crack in a rectangular plate – not least showing that our results are arguably more accurate than the best results found in the technical literature. We restrict our present assessments to the CTOD evaluation of SIFs of straight and star shaped cracks in the open domain, as the local stress state around a crack is actually the most relevant – and critical – issue to be adequately assessed. Nevertheless, we borrow an example from [16] to illustrate an application to a mixed mode problem.

2 Stress intensity factors based on crack tip opening displacements

Since we are dealing with very accurate numerical approximations, we apply the CTOD technique to express modes I and II SIFs in terms of the exact Westergaard's function [4] for the relative opening and slip displacements, $\Delta u_\perp$ and $\Delta u_=$, of two opposite points of the crack face ideally – but not necessarily – as close to the tip as possible,

$$(K_I, K_{II}) = \lim_{r\to 0} \frac{G\sqrt{\pi a}}{2\,(1-\nu)\,\Im\left(\sqrt{z^2-a^2}\right) \mp y\Re\left(\dfrac{z}{\sqrt{z^2-a^2}}\right)} \left(\Delta\nu_\perp, \Delta \mathrm{u}_=\right), \quad z = a-x+iy,\ r = |z-a|, \tag{1}$$

as for plane strain state, for comparison with a straight crack of semilength a and the tip located on the right, as in any of the configurations shown in Fig. 1 and such that the abscissa x increases from the crack tip to the left. We also suggest the second-order approximation of this expression

$$(K_I, K_{II}) = \lim_{r\to 0} \frac{G\sqrt{\pi}\sqrt{r+x}}{2\,(1-\nu)\,(r+x)\left(1+\dfrac{1}{4a}\,(r-2x)\right) \mp \dfrac{y^2}{2r}\left(1+\dfrac{3r}{4a}\right)} \left(\Delta\nu_\perp, \Delta \mathrm{u}_=\right) + O\left(\frac{r}{a}\right)^2, \tag{2}$$

with two terms of the expansions [17] of the real and imaginary parts of the Westergaard's functions indicated in eq. (1). The technical literature usually only shows the first-order approximation, as for $y \to 0$ and $r/a \to 0$ [6, 18].

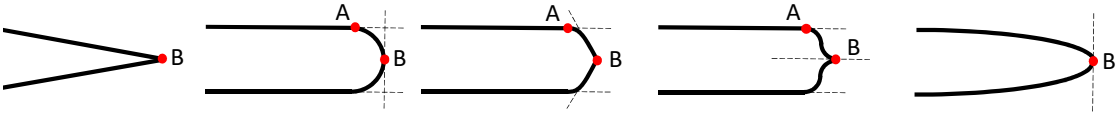

Figure 1. Five possible local geometric configurations of the crack tip

The CTOD technique involves much lower computational costs than in terms of the J integral, as no stress results at internal points need to be evaluated, although it is possibly less reliable [16], since displacement results at boundary nodal points that are too close to the crack tip depend on the crack tip initial configuration and are liable to oscillate [15]. This will be elucidated by means of a few numerical examples.

2.1 Straight crack in the open domain

Our presently available boundary element code models the crack's faces as separated surfaces no matter how close they are to each other [13, 16]. Modeling two crack surfaces as geometrically collapsed is in reach of our developed tools, as all hypersingular integrals required in such numerical implementation are already part of our code, which gives stress results at internal points within machine precision [13]. However, we are not so much in a hurry to ultimate this particular implementation as collapsed crack surfaces are actually a physical impossibility and we are able to account mathematically for distances in the nanometer range, as illustrated in the following.

The problem of a straight crack in the open domain was analytically solved by Westergaard and, since such solution is just an idealization, we can presently simulate it only approximately. Several relatively successful

attempts using almost collapsed ellipses, for instance, have already been carried out by the authors [9, 10, 14, 16]. We initially simulate a straight crack as the diamond shape on the left in Fig. 2 – and the triangular crack tip configuration shown in Fig. 1 –, with each straight face of a quarter of the crack modeled with either 24 quadratic or 12 quartic elements, thus with a total of 192 nodes (not taking advantage of symmetries). This – as well as most cases reported in the literature – is a problem with Neumann boundary conditions. We actually have zero tractions applied to the boundary but body forces corresponding to the indicated stress state at infinity to be considered in the numerical implementation. We use $2b = 0.0015$, $2a = 19.06 \Rightarrow b/a \approx 7.87 \times 10^{-5}$ and Poisson's ratio $\nu = 0.25$. The relevant information are just b/a and ν.

Figure 3 presents the results for five numerical simulations in which the distance between two adjacent nodes along a crack face increases from crack tip to the middle with geometric ratios $1.1, 1.2, 1.3, 1.4$ and 1.5. This leads to the closest distances from a node to the crack tip indicated in the first row of Table 1 and corresponding extremely small distances between opposite nodes indicated in the second row. The mode I reference solution in Fig. 3 is $K_I = \sigma\sqrt{\pi a}$ [19] as for a straight crack with zero opening. The graphs of Fig. 3 present on the left relative errors in comparison with the target value and on the right the relative results for K_I evaluated according to eq. (1) for pairs of opposite crack face nodes located along the relative distance $\approx 0 < r/a \leq\approx 0.01$. SIFs evaluations using the two term approximation of eq. (2) are essentially the same, in the present case, as well as if one considers just one term, as usually preconized. There is a plateau of best results for $r/a \approx 10^{-3} \sim 10^{-2}$ also corresponding to relative errors approximately $10^{-5} \sim 10^{-3}$. Observe that using large ratios of increasing node spacing – too abrupt interdistance changes of 40% and 50% – does not lead to better results even though the nodes closest to crack tip are indeed very close, as given in the Table.

Table 1. Distances of the first node counting from crack tip as well as from opposite node for the crack on the left in Fig. 2 modeled with the indicated ratios of increasing node spacing

Spacing ratio	1.1	1.2	1.3	1.4	1.5
Distance to crack tip	9.925×10^{-3}	3.016×10^{-4}	9.704×10^{-6}	3.690×10^{-7}	1.681×10^{-8}
Distance between nodes	1.562×10^{-4}	4.748×10^{-6}	1.527×10^{-7}	5.808×10^{-9}	2.647×10^{-10}

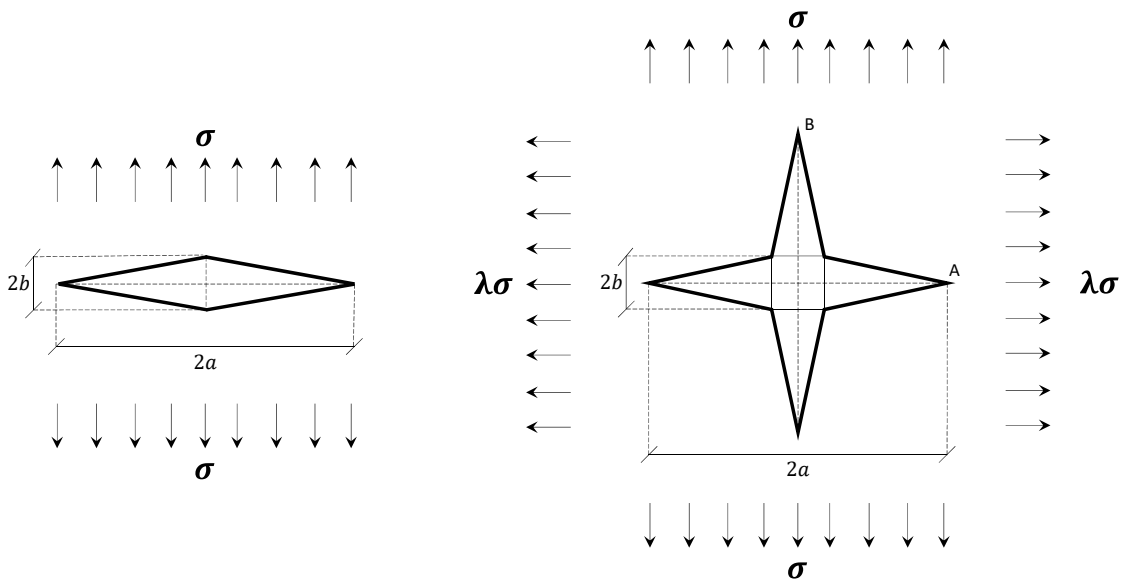

Figure 2. Diamond and star shaped cracks in the open domain for $b/a \rightarrow\approx 0$

Results for quadratic elements and the same mesh discretization are about one order of magnitude less accurate [15]. We used $ng = 8$ Gauss-Legendre points for the numerical evaluation of the regular parts of the integrals, which is particularly important for the ratio 1.5, for instance. (Good convergence is checked when comparing $ng = 8$ and $ng = 10$.) Our node generation algorithm considers how the distance between nodes vary (and not element sizes) such that the Jacobian of coordinates transformation is not constant even in the case of a straight element. The issue of how relatively close a source point must be to a boundary element in order to be considered close – and then have the integrals adequately dealt with, according to Dumont [20], – has also been checked in the present numerical assessments, and we find out that actually no special treatment is needed when such a rela-

tive distance is larger then two. We have also carried out an h-convergence assessment of the proposed numerical model and obtained precision errors demonstrably smaller than the ones the present graphs display.

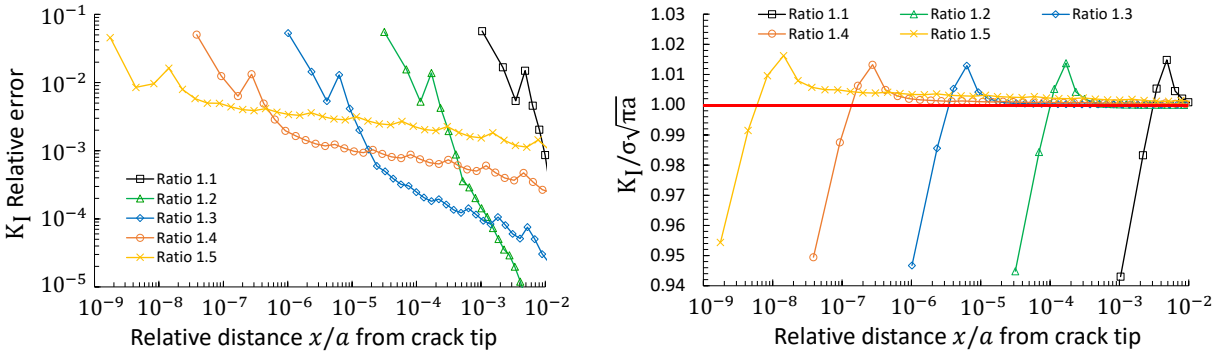

Figure 3. K_I relative errors (left) and values (right) for the crack problem on the left in Fig. 2 for the triangular crack tip configuration of Fig.1 and different ratios of internode increasing distances from crack tip

2.2 Straight crack in the open domain with modified tip configurations

In this study we use the same basic proportion $b/a \approx 7.87 \times 10^{-5}$ and material property $\nu = 0.25$ of the previous example but keep the crack faces parallel while trying to accommodate the tip shape in different ways, as shown in Fig. 1. In this figure, the *triangular* tip is just the tip of the previous model with a diamond shaped crack, which is used for the sake of comparison with the other indicated geometries. The *doubly smooth* tip has nodes A and B as the extremities of a unique boundary element that can be quadratic, cubic, quartic and so on, with the indicated prescribed tangents and zero tangent derivatives leading to equation systems for the location of the internal nodes. The *smooth/inclined* tip is similar to the previous one, except that the tangent at point B is not prescribed but rather the tangent's derivatives are set equal to zero. Finally, the *smooth/parallel* tip has horizontal tangents and higher derivatives are set equal to zero in such a way that the vertical location of the internal nodes be determined. Owing to the required inflection the latter geometry only works with cubic and higher order elements. For the sake of completeness of the analyses we also consider the *elliptical* shape on the right in Fig. 1, which has been the first shape considered in our path of dealing with fracture mechanics problems [9, 10, 14, 16]. In this latter simulation the nodal points are located along an ellipsis of half axes (a, b) and the justification is that we already expect a collapsed elliptical shape to be the most natural one coming from Westergaard's developments. The disadvantage of this model is that the resulting geometry with quadratic, cubic or quartic elements actually leads to angulations between elements, which may cause disturbances of the local stress field.

Figure 4 shows the comparisons for the crack configurations of Fig. 1 using quartic boundary elements and numerical integrations with $ng = 8$. Results with triangular and elliptical crack tip configurations present the lowest errors. The doubly smooth and the smooth/inclined tip configurations do not seem to be competitive.

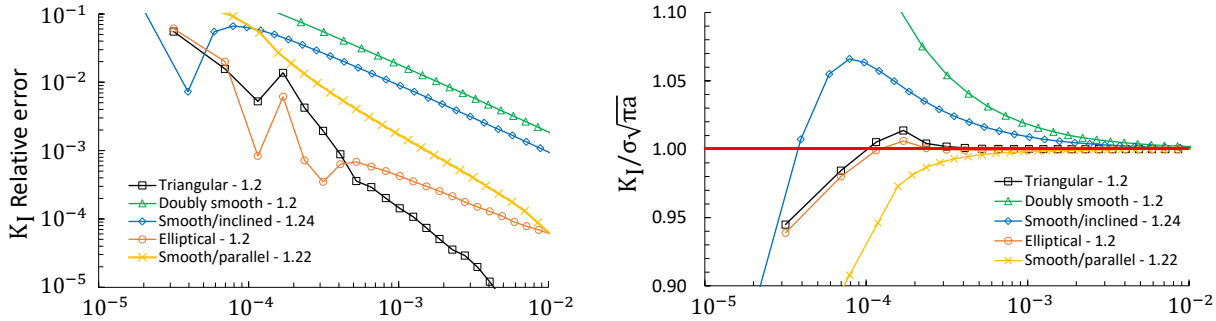

Figure 4. K_I relative errors (left) and values (right) for the crack on the left in Fig. 2 and the crack tips of Fig. 1

2.3 Star shaped crack in the open domain

The star shaped crack of Fig. 2 is modeled with 48 nodes along each of the eight faces (no advantage taken of symmetries) and triangular crack tips, also considering $\nu = 0.25$, thus much the same as for the previous example, although with still smaller relative opening $b/a = 10^{-5}$. The literature reference SIF values for $b/a = 0$ are

$K_{IA} = \sigma\sqrt{\pi a}(1.0863 - 0.2227\lambda)$ and $K_{IB} = \sigma\sqrt{\pi a}(-0.2227 + 1.0863\lambda)$ at tips A and B [19]. Figure 5 shows SIFs results for the stress ratio $\lambda = 0$ using the CTOD eq. (2) with just one term (left), that is, considering $y = 0$ and $r/a = 0$, as well as the full eq. (1) (right) at tip A for simulations with quadratic and quartic elements and a few different internode space increasing ratios. Our best results are consistently lower than the reference ones.

Error results for different λ ratios of stress application in Fig. 2 – as compared with Tada et al [19] – are shown in Fig. 6 for the crack tips A and B and using the CTOD full eq. (1). We use quadratic elements and internode distance increasing ratio 1.3. The results displayed at crack tip A for $\lambda = 0$ are the same ones of Fig. 5 but corresponding values cannot be shown for crack tip B. In fact, we should expect that some of the crack branches close depending on the stress ratio λ, which is not considered Tada et al [19] in terms of the range of validity of λ. One of our next analyses shall be the consideration of different values of the Poisson's ratio ν, which influences the crack tip openings and is duly taken into account in both eqs. (1) and (2).

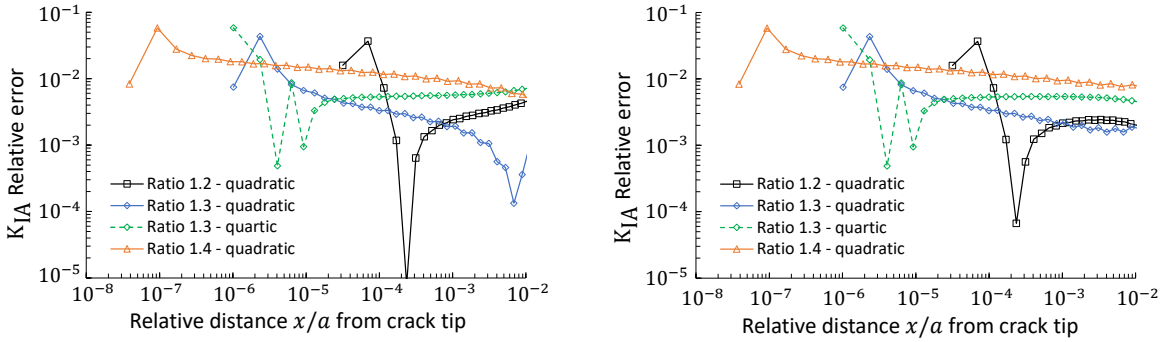

Figure 5. SIFs results using the CTOD eq. (2) with one term (left) as well as the full eq. (1) (right) at tip A of the star shaped crack of Fig. 2 for simulations with quadratic and quartic elements

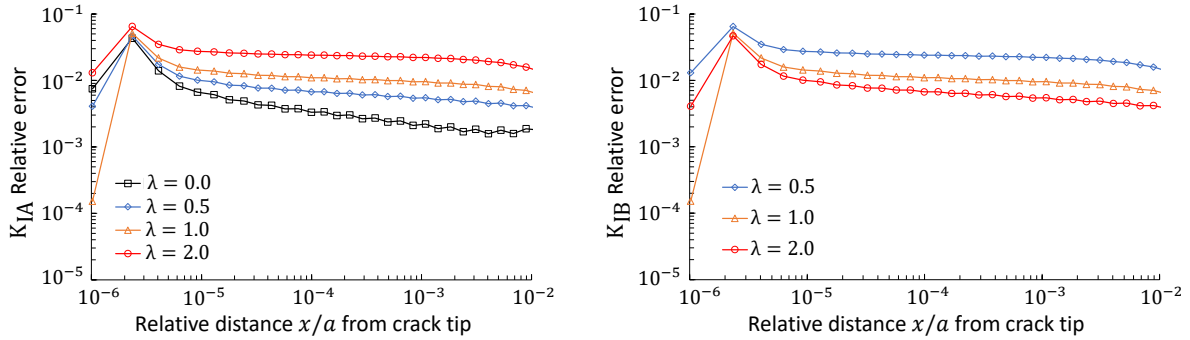

Figure 6. Relative K_{IA} and K_{IB} errors for the star shaped crack of Fig. 2 under different λ loading combinations using quadratic elements with the internode distance increasing ratio 1.3

2.4 Mixed mode analysis of an inclined edge crack [16]

This example is reproduced from Dumont and Amaral Neto [16] in order to just illustrate an application to a mixed mode problem. Namakian et al [21] analyzed a rectangular plate of dimensions $444.5 \times 177.8mm^2$ using two quite similar meshless implementations [results here referred to as (a) and (b)], with normalized modes I and II SIFs K_I and K_{II} compared with another meshless model by Zhuang et al [22] as well as with the key reference results by Murakami [23]. There is a 45^0 degree slanted crack of (very large) length $177.8/\sqrt{2}mm$ starting $177.8mm$ from one border, so that two pieces of preserved $177.8 \times 177.8mm^2$ squares are kept before and after the crack formation. The plate is submitted to uniform normal stress along its short edges for plane strain state and Poisson's ratio $\nu = 0.25$. The (K_I, K_{II}) results found by these authors were apud [21] respectively $(1.830, 0.814)$ [21](a), $(1.833, 0.819)$ [21](a), $(1.778, 0.799)$ [22] and $(1.856, 0.834)$ [23].

We ran two analyses, for edge openings $2 \times 10^{-3}mm$ and $2 \times 10^{-5}mm$. The plate was simulated with $8 + 20 + 8 + 20 = 56$ equally spaced quadratic elements along the borders and 22 quadratic elements along each of the crack faces, for internode distance increasing from crack tip by a factor 1.15: the distance from crack tip to the first node was $0.04034mm$ (≈ 0.00032 relative to crack length).

CTOD results in terms of eq. (2) with one term for opposite points along the crack face showed to be quite

stable for a relative distance $r/a \approx 0.011$ from crack tip, node 141, which corresponds to the opposite nodes 128 and 154, $2.204 \times 10^{-5} mm$ and $2.204 \times 10^{-7} mm$ apart for the edge openings $2 \times 10^{-3} mm$ and $2 \times 10^{-5} mm$, respectively. The corresponding (K_I, K_{II}) values are $(1.845, 0.824)$ and $(1.837, 0.824)$, which are confronted in Table 2 with the previously reported results. Our results lie between the results obtained by Namakian et al [21] and Murakami [23] and are most probably the more reliable ones.

Table 2. Percentage errors in comparison with literature results [21–23] (from [16]).

	[21](a)	[21](b)	[22]	[23]
K_I	0.82, 0.38	0.65, 0.22	3.8, 3.3	-0.59, -1.0
K_{II}	1.2	0.61	3.1	-1.2

3 Conclusions

This short communication illustrates the application of the consistent collocation boundary element method unaltered to two-dimensional problems of linear fracture mechanics. The implemented code deals with singularities of any degree of severity for any topological configurations, as illustrated in the first example for nodal points at opposite crack faces that are just nanometers apart. We have already implemented the evaluation of stress intensity factors in terms of the J-integral for the mode I case. Our focus here was the technique of crack tip opening displacements, which is very expedite and easily generalizable although in principle more liable to geometric peculiarities. We dedicated most part of our developments to the assessment of the adequate geometric configuration of the crack tip for the simplest problem proposed and solved by Westergaard. In fact, the local geometry and stress state are the relevant aspects to be dealt with, since taking the far field effect into account is a lesser issue.

Since we have complete control of the computational precision (machine precision is in reach of our developments), we are able to address the approximation aspects of the crack tip opening displacement technique itself and the eventual influence of a material's Poisson's ratio on the stress intensity factor. We show that multiple cracks can be seamlessly simulated and – owing to space restrictions – only in passing illustrate the case of a mixed mode problem. We have already showed that there is no ill-conditioning related to crack faces that are just nanometers apart. The present implementation may be easily generalized for combination with cohesive elements and there are already developments in progress for the simulation of crack propagation. We have already experience in dealing with the formation of plastic zones around crack tips in the frame of a hybrid boundary element formulation in terms of generalized Westergaard functions and think that such developments in the present framework are perfectly feasible and more straightforward.

Acknowledgements. This project was supported by the Brazilian agencies CAPES and CNPq.

Authorship statement. The authors hereby confirm that they are the sole liable persons responsible for the authorship of this work, and that all material of the present paper is the property (and authorship) of the authors.

References

[1] C. E. Inglis. Stress in a plate due to the presence of cracks and sharp corners. *Transactions of the institute of Naval Archtects*, vol. 55, pp. 219–241, 1913.
[2] A. A. Griffth. The phenomena of rupture and flow in solids. *Philosophical Transactions*, vol. 221, pp. 163–198, 1920.
[3] G. R. Irwin. Onset of fast crack propagation in high strength steel and aluminum alloys. *Sagamore Research Conference Proceedings*, vol. 2, pp. 289–305, 1956.
[4] H. M. Westergaard. Bearing pressures and cracks. *Journal of Applied Mechanics*, vol. 6, pp. 49–53, 1939.
[5] G. R. Irwin. Analysis of stresses and strains near the end of a crack traversing a plate. *Journal of Applied Mechanics*, vol. 24, pp. 361–364, 1957.
[6] D. S. Dugdale. Yielding of steel sheets containing slit. *Journal of Mechanical Physics Solids*, vol. 8, pp. 100–104, 1960.
[7] J. R. Rice. A path independent integral and the approximate analysis of strain concentration by notches and cracks. *Journal of Applied Mechanics*, vol. 35, pp. 379–386, 1968.

[8] T. A. Cruse and W. Van Buren. Three dimensional elastic stress analysis of a fracture specimen with an edge crack. *International Journal for Fracture Mechanics*, vol. 7, pp. 1–15, 1971.
[9] N. A. Dumont and A. A. O. Lopes. On the explicit evaluation of stress intensity factors in the hybrid boundary element method. *Fatigue & Fracture of Engineering Materials & Structures*, vol. 26, pp. 151–165, 2003.
[10] N. A. Dumont and E. Y. Mamani. Generalized Westergaard stress functions as fundamental solutions. *CMES – Computer Modeling in Engineering & Sciences*, vol. 78, pp. 109–150, 2011.
[11] N. A. Dumont, E. Y. Mamani, and M. L. Cardoso. A boundary element implementation for fracture mechanics problems using generalized Westergaard stress functions. *European Journal of Computational Mechanics*, vol. 27:5-6, pp. 401–424, 2018.
[12] N. A. Dumont. The boundary element method revisited. *Boundary Elements and Other Mesh Reduction Methods XXXII*, vol. 50, pp. 227–238, 2010.
[13] N. A. Dumont. The collocation boundary element method revisited: Perfect code for 2D problems. *International Journal of Computational Methods and Experimental Measurements*, vol. 6, pp. 965–975, 2018.
[14] O. A. Amaral Neto. Consistent application of the boundary element method to fracture mechanics problems (in Portuguese). Master's thesis, Pontifical Catholic University of Rio de Janeiro, Rio de Janeiro, Brazil, 2020.
[15] O. A. Amaral Neto. *General fracture mechanics problems analyzed with the consistent boundary element method*. PhD thesis, Pontifical Catholic University of Rio de Janeiro, Rio de Janeiro, Brazil. (In progress), 2023.
[16] N. A. Dumont and O. A. Amaral Neto. Machine-precise evaluation of stress intensity factors with the consistent boundary element method. *International Journal of Computation Methods and Experimental Measurements*, vol. 9, n. 2, pp. 141–152, 2021.
[17] M. L. Williams. On the stress distribution at the base of a stationary crack. *Journal Applied Mechanics*, vol. 24, pp. 109–114, 1957.
[18] D. J. Unger. *Analytical Fracture Mechanics*. Dover, 1995.
[19] H. Tada, P. C. Paris, and G. R. Irwin. *The Stress Analysis of Cracks Handbook*. Paris Productions, 2000.
[20] N. A. Dumont. The boundary element method for 2d problems of potential and elasticity: Conceptually consistent formulation, a convergence theorem and numerical evaluations within machine precision. *Engineering Analysis with Boundary Elements*. (To be submitted), 2022.
[21] R. Namakian, H. M. Shodja, and M. Mashayekhi. Fully enriched weight functions in mesh-free methods for the analysis of linear elastic fracture mechanics problems. *Engineering Analysis with Boundary Elements*, vol. 43, pp. 1–18, 2014.
[22] X. Zhuang, C. Augarde, and S. Bordas. Accurate fracture modeling using meshlessmethods, the visibility criterion and level sets: formulation and 2d modeling. *International Journal for Numerical Methods in Engineering*, vol. 86, pp. 249–268, 2011.
[23] Y. Murakami. *Stress Intensity Factors Handbook*. Pergamon Press, 1987.
[24] T. H. Baek and C. P. Burger. Accuracy improvement technique for measuring stress intensity factor in photoelastic experiment. *KSME Journal*, vol. 5, pp. 22–27, 1991.